京都大学防災研究所年報 第 56 号 B 平成 25 年 6 月
Annuals of Disas. Prev. Res. Inst., Kyoto Univ., No. 56 B, 2013

Study on Characteristic Analysis of Closed-type Sabo Dam with a Flap due to Dynamic Force of Debris Flow

Yeonjoong Kim(1), Hajime NAKAGAWA, Kenji KAWAIKE, and Hao ZHANG

(1) Graduate School of Engineering, Kyoto University

Synopsis

In recent years, many research studies have examined efficient function of sabo dams, which have a great impact on ecology and landscape. In that research, attention to the aspect of analysis of impact force associated with debris flow is still lacking. The front part of the flow is very important and complex in the case of debris flow where there is an accumulation of large boulders. It is important to control or dampen the energy of the frontal part of a debris flow for the safety of the downstream area because the impact pressure of debris flow is much greater than that of clear fluid. Therefore an alternative design and its resistance against debris flow impact force deserve investigation. The objectives of this study are to analyze, firstly, the function of the proposed closed-type dam with a flap, then to compare the vertical pressure distribution and total pressure with other types of available dams and finally, to determine the empirical coefficients of the hydrodynamic and solid collision models. This comparison demonstrates the future importance of the proposed sabo dam. The results from the experimental data clearly show that the proposed dam type has the ability to capture more sediment sustaining less force than the without flap dams under the same debris flow. Furthermore, the empirical coefficients of hydrodynamic and solid collision models were proposed and compared with available coefficients.

Keywords: debris flow, closed-type flap dam, impact force, total pressure

1. Introduction

Debris flows are common in mountainous areas throughout the world, which contain various amounts of mud, sand, gravel, boulders, and water. They occur when water mobilizes large volumes of loose mud, rock, and other debris. It is generally accepted that debris flow disaster occurs in high mountainous areas far away from modern cities. Recently, this disaster simultaneously occurs in multiple locations between the high mountainous areas and the low mountainous areas in urban areas (Kim et al. 2013).

The debris flow disasters that occurred at Mt. Umeyon in downtown Seoul, Korea 2011 are shown in Photo 1 (a), photo (b) shows extensive damage to that the apartment in Caraballeda due to a passage of a debris flow front of at least 3.5m in height (Larsen et al. 2001). These disasters illustrate the destructive power of the high-velocity fluid as well as debris flow and flash floods on alluvial fans inundating coastal communities, causing severe property destruction, and resulting in a death toll estimated at 19,000 people. The debris flow disaster leads to massive property damage and casualty of life. Therefore, to estimate the disastrous effects, it is necessary to accurately understand, evaluate, quickly respond to the risks, and mitigate damage by establishing an effective measure.

(a) Mt. Umeyon (photo courtesy: PRESSian) (b) Caraballeda

Photo 1 Debris flow disaster

In recent years, many researchers have experimented with the efficiency of sabo dams having a great impact on ecology and landscape. Such dams are also surcharged with the impulsive forces of the debris flow. The front part of the flow is important and complex in debris flow where big boulders accumulate. It is important to control or dampen the energy of the front part of a debris flow for the safety of the downstream area because the impact pressure of debris flow is greater than that of clear fluid. Fig. 1 (a) shows typical features of a debris flow longitudinal section (Pierson, 1986) and Fig. 1 (b) shows the various functions of a sabo dam (MLIT, Japan. 2011). Therefore, we have to consider both characteristics of debris flow and sabo dam with an effectively counterplan for mitigate the debris flow disaster.

Much research is being carried out to improve the function of sabo dams as well as to clarify the impact force of debris flow based on field observations, laboratory experiments (i.e. large and small scale), and numerical simulations. A few field experiments have been conducted such as Okuda et al. (1978), Suwa and Okuda (1983), and Hu et al. (2011). In addition to these Hu et al. (2011) reported an in-situ test of debris flow impact at Jiangjia Ravine, and introduced a simple approach to separate two components of the impact force into fluid pressure and grain-impact loading. In those studies, preliminary analyses were made to determine the relationships of mean velocity versus hydrodynamic pressure, and hydrodynamic pressure versus grain impact loading from the measured data due to the subtracting the fluid pressure from the total impact loading.

Many small-scale laboratory experiments have been performed in order to develop theoretical models for the calculation of impact force. Mizuyama (1979) separated the impact force of debris flow into the fluid force and impact force of boulder.

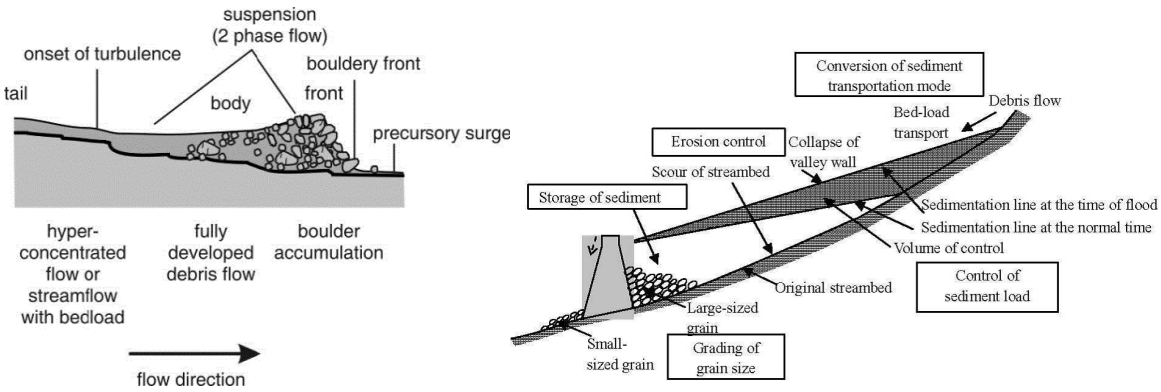

(a) Debris flow surge (b) Various functions of a sabo dam

Fig. 1 Sketch of the characteristics of debris flow and functions of a sabo dam

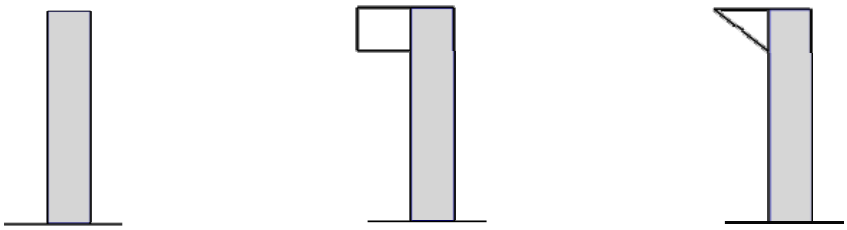

(a) Without flap (i.e. typical type) (b) With flap-R (c) With flap-T

Fig. 2 Sketch of closed-type dams

According to the paper, the impact force on a sabo dam (i.e. without flap) is described with hydraulic theories and the theory of complete sphere elasticity was assumed so that the impulsive force of the boulders could be derived. Scheidl et al. (2012) analyzes the impact forces of granular and viscous debris flow and discusses the observations of single, short time impacts of large particles, significantly exceeding the peak pressure values. However, there have been very few studies that discuss how debris flow is influenced by the shape of a sabo dam. Shieh et al. (2008) designed a new form of sabo dam by changing the geometric shape of the upstream dam surface to reduce the impact force of the debris flow, with enhanced stability and reduced concrete mass being the anticipated outcomes. Their study showed that the curved dam experiences less impact force than other dams under the same debris flow condition, demonstrating the importance of curved geometry for a well-designed sabo dam. Huang et al. (2007) applied the theory of elastic collision to devise a boulder collision impact model with four types of dams. Recently, Shibuya et al. (2012) presented the load of debris flow with woody debris for an open type steel frame check dam structure. Likewise, understanding the behavior and mechanism of debris flow and the study of preventive measures are very important in order to manage the sediment disaster in the river basin and prevent downstream hazards. Preventive measures require the consideration of various plans and involve the evaluation of hydrological, hydraulic, grain size distribution, topographical and other parameters.

The objectives of this study are to analyse the working principle of proposed closed type dams (i.e. in Fig. 2 (b) and (c)) with a flap over typical type dam (i.e. dam without flap as shown in Fig. 2 (a)), to propose the most suitable flap shape (i.e. rectangular or triangular shape) based on apparent characteristics, and to determine the empirical coefficients of the hydrodynamic and solid collision model.

Experiments were conducted to investigate total pressure (combination of impact due to the collision, static and dynamic pressures) of both flows under the conditions of closed-type dam without flap and that with a flap. In the experiments, total pressure associated with major debris flows was recorded in real time by a system consisting of four dynamic pressure sensors (i.e. strain gages) installed at the dam. As stated above, the applied force of debris flow is usually determined by field observations, laboratory experiments and numerical simulations. But it is very difficult to estimate the applied force due to the impact collision because the debris flow is composed of many different sizes and fractions of sediment, which makes it difficult to estimate the actual contact area. So, the average value of the total pressure by the maximum value of the impact collision is determined experimentally by conducting several experiments under the same conditions.

In all the experiments, the parameters such as the flow pattern, the surface velocity between the debris flow and clear water, the total pressure, mass ratio of debris, median grain diameter of debris flow, and the uplift pressure were measured to compare the function of each check dam under the two different bed sediments. The empirical coefficients of the hydrodynamic and solid collision models were also determined and compared with the available values of those coefficients. Furthermore, observations of the load behavior of debris flow, the velocity, the average of maximum total pressures, the uplift pressure due to the impact collision, the vertical distribution of total pressure on the dams and the ability of the proposed dam to sustain such forces, are also discussed.

2. Debris flow impact model

Several models have been developed to estimate the impact force of debris flow against barriers. However, it is difficult to decide the impact force due to the diversity of substances composing the debris flow (i.e. water, mixtures of granular and fine particles in water and boulders) and the conditions of dam (e.g. flexibility and properties). The impact force of debris flow has been mainly described by hydraulic and solid collision models. The hydraulic models are further separated into hydrostatic and hydrodynamic models. Based on observations and theoretical consideration, different models have been developed for estimation of the debris flow impact force.

2.1 Hydrostatic model

The hydrostatic models by Lichtenhahn (1973) and Armanini (1997) are useful because they require only the debris flow height, and the height of the structures is often taken as debris flow height for checking dam design purposes. In general, the hydrostatic formula can be written as:

$$P_{\max} = k_p \rho_d g h \tag{1}$$

where $P_{\max}$ = the maximum debris flow impact pressure, k_p = the empirical factor, ρ_d = the density of debris flow, g = the acceleration of gravity, and h = the depth of debris flow. The maximum impact pressure is not related to statistical considerations, but to the maximum pressure value in the load distribution on the structure (Hübl et al. 2009). Lichtenhahn (1973) proposed kp values between 2.8 and 4.4. Armanini (1997) found a maximum static debris flow impact pressure exceeding roughly 5 times the hydrostatic pressure. Scotton and Deganutti (1997) measured the impact on an obstacle and proposed k_p values between 2.5 and 7.5 from the laboratory experiment.

2.2 Hydrodynamic model

The hydrodynamic formulas are based on the impulse theorem. The phenomenon of debris flow impact against an obstacle has been analysed in scientific literature; many empirical and non-empirical relations can be found for the calculation of the dynamic thrust.

$$P_{\max} = k_p \rho_d v^2 \tag{2}$$

$$F_{\max} = k_f \rho_d A v^2 \tag{3}$$

where $P_{\max}$ = the maximum debris flow impact pressure, k_p and k_f = the empirical factors, ρ_d = the density of debris flow, v = the velocity of debris flow, $F_{\max}$ = the modulus of the impacting force, and A = the area of the section involved in the phenomenon and whose height should be considered as the height of the debris flow front. The empirical factor value depends on the flow type. For laminar flow and fine grained material, Zhang (1993) recommends the pressure of empirical values between 3.0 and 5.0 based on field measurements at the Jiangjia Gully station. Bugnion et al. (2011) proposed that the pressure of empirical coefficient kp approximately in the range between 0.4 and 0.8 appear to be appropriate for objects with size of the same order of magnitude as the flow heights. Canelli et al. (2012) estimated the force of empirical coefficient between 1.5 and 5.0 by a laboratory experiment with a small scale channel. Watanabe and Ikeya (1981) proposed that the force of empirical value changes with flow material; for clear water, k_f has been found to be between 1 and 2, and for bentonite, k_f = 2.0 as well as value of 1.5 by Hungr et al. (1984). Besides, when designing a sabo dam in Japan, it is usually done using Eq. (3) (Yamamoto et al. 1998).

2.3 Solid collision model

Conventional contact mechanics is mainly concerned with static contact although it has been extended to approximate solutions when impact is involved. For spheroidal surfaces, Hertz theory is used to obtain the force deformation relation needed to calculate the duration of impact and the maximum indentation. According to Jackson and Do (1969), for the case of impact between two spheres of mass m_1, and m_2, investigations show that the duration of impact, i.e., the time during which the spheres remain in contact, is very long in comparison with the period of lowest mode of vibration of the spheres. Vibrations can therefore be neglected, and it can be assumed that

the force-displacement relation established for static conditions holds during impact. The compressive force is basically a power law written as:

$$F = n\alpha^{3/2}$$
$$\beta = \sqrt{\frac{16R_1R_2}{9\pi^2\left(k_1+k_2\right)^2\left(R_1+R_2\right)}}$$
$$k_1 = \frac{1-\upsilon_1^2}{\pi E_1},\quad k_2 = \frac{1-\upsilon_2^2}{\pi E_2} \qquad (4)$$
$$\alpha = \left(\frac{5(v_1+v_2)^2}{4\beta\gamma}\right)^{2/5},\quad \gamma = \frac{m_1+m_2}{m_1m_2}$$

where F = the compressive force (i.e. the force that acts during the period of impact between the spheres), υ_1 and υ_2 = Poisson's ratio, E_1 and E_2 = Young's moduli, v_1 and v_2 are the velocities of the colliding particles, R_1 and R_2 = the radii of spherical surfaces of the two bodies at the point of contact, and m_1 and m_2 = the mass of sphere. Mizuyama (1979) calculated the impact load between sabo structure (relates parameters with subscript 1 in above equation) and debris flow (relates parameters with subscript 2 in above equation) based on different assumed values of parameters used in equation 4. Mizuyama assumed the Young's modulus of material forming the sabo structure $E_1 = 5\times10^8$ kg/m^2 (as of concrete) and the materials forming the debris flow $E_2 = 2\times10^9$ kg/m^2 (as of stone), Poisson's ratios of sabo structure material υ_1 =1/6 (as of concrete) and material of debris flow υ_2 =1/5 (as of stone), and v_1 is equal to zero (since sabo structure is stationary) so that $v_1 + v_2$ is taken as equal to v_2 (the approaching velocity of debris flow). The impact load is rewritten using the properties of concrete (i.e. sabo dam) and large boulder as:

$$F_{\max} = k_f\, 48.2 v_2^{1.2} R_{\text{boulder}}^2 \qquad (5)$$

where k_f = the control empirical factor, v_2 = the approaching velocity of debris flow, and R_{boulder} = the radius of the boulder.

3. Laboratory experiment

To clarify the characteristics of debris flow in comparison with clear water as well as to compare the functions of the proposed dams with typical dam (i.e. without flap), experiments were conducted in a flume located at the Ujigawa Open Laboratory (UOL) of the Disaster Prevention Research Institute (DPRI), Kyoto University, Kyoto, Japan.

3.1 Working principle of sensor

The dynamic pressure measurement system is produced by a Japanese company, Kyowa. The measuring system was composed of four dynamic pressure sensors (diaphragm type), sensor Interface (PCD-300B), and four channels of Adaptor and Note-PC by the dynamic data acquisition software (DCS-100A) as shown in Fig. 3. These sensor transducers have a bridge of strain gages inside, achieving ultra-thin compact structure. Kyowa strain gages are available for the measurement of various types of strain, from static to dynamic strain and impact-initiated strain. Strain gages are used not only for stress measurement but also as sensing elements for various transducers owing to their excellent repeatability and linearity. Dynamic strain is a strain whose magnitude changes as time passes or which is initiated by vibration or impact. Since ever-changing strain cannot be read out on analog and digital indicators, a data recorder was used to obtain the

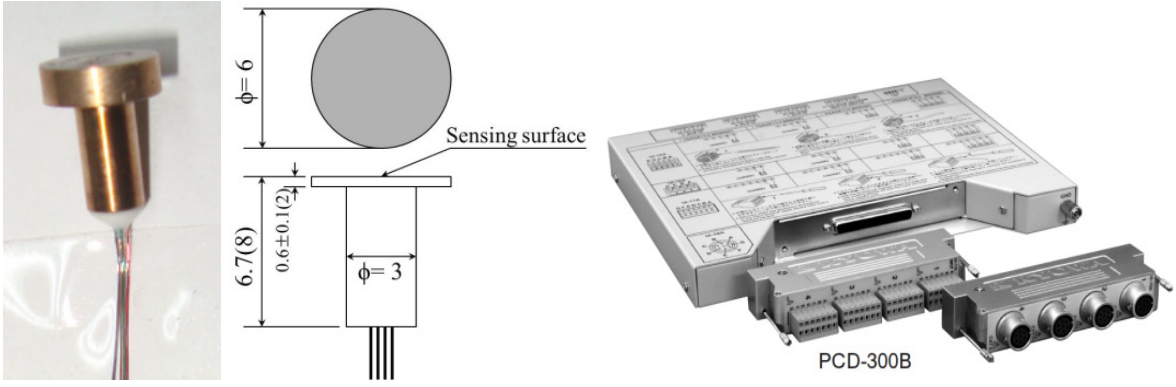

Fig. 3 Dynamic pressure sensor and interface with four channels (unit: mm)

detected data. Table 1 shows the specification of the sensors. Pressure sensors are measuring devices that produce an output signal proportional to the applied dynamic pressure and the total pressure is calculated by the following relation as proposed by the company, Kyowa.

$$Pressure(\mathrm{Pa}) = \frac{\left(Strain\ \ amplifier's\ \ output,\ \ \varepsilon \times 10^{-6}\right)}{\left(Rated\ \ output\ \ on\ \ labe,\ \ \mathrm{mV/V}\right)} \times \frac{Capacity(\mathrm{Pa})}{\left(2000 \times 10^{-6}\ /\ \mathrm{mV/V}\right)} \quad (6)$$

Compression pressure values are used to measure the positive force along a single axis. The information from the sensor monitor is then transferred to a recorded or other computerized data collection system. The sampling frequency (f_{scan}) adopted in the experiments is 500 Hz based on Nyquist-Shannon sampling theorem as shown in Eq. (7), and is able to show the dynamic variation within every 0.002 s.

$$f_{scan} = 2f_{max},\ \ (f_{max} = \frac{v_{avg}}{d_{max}}) \quad (7)$$

where v_{avg} = the average velocity of debris flow and d_{max} = the maximum grain diameter.

3.2 Experimental setup

3.2.1 Experiment for hydraulic characteristic

The experiments confirmed the characteristic of debris flow and observed the energy dissipation phenomenon near the dam. Only two types of closed dams (i.e. without and with flap-R) under the two flow conditions i.e., the clear water flow and the debris flow were tested. To clarify the characteristic of debris flow, hydraulic model tests with clear water were performed for comparing the flow profile and total pressure in a rectangular flume that was 100 cm long, 15 cm wide, and 40 cm high. At a distance of 60 cm from its downstream end, a vertical gate was installed as shown in Fig. 4. The walls and bottom are made of transparent smooth acrylic plank, which allows for lateral observation. At the dam section, the flume is equipped with a smooth gate that can open by hand. The flow was filmed with a digital video camera (Sony: HDR-CX560) placed on the side of the channel. The efficiency of the two types of dam with plan-1 (without and with flap-R structure) is discussed comparing the total pressure and flow profile near the dam.

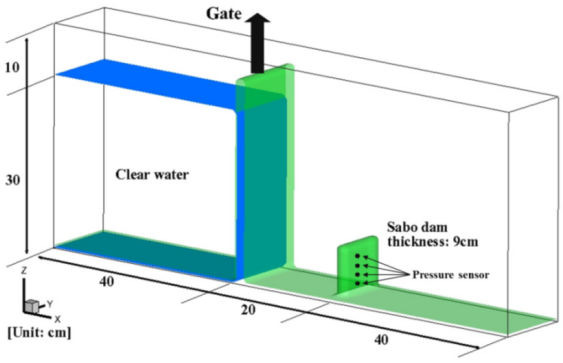

Fig. 4 Experimental set-up for dam-break upstream of the proposed dam

3.2.2 Experiment for debris flow

The debris flow experimental facility consists of a 5.0 m long horizontal smooth flume with a rectangular section 10cm wide and 14cm high. One side of the walls is made of transparent glass and the other side is opaque made of PVC. The slope of the flume is set at 18°. The sabo dams were built using

Table 1 Specification of the sensor

	Sensor-A	Sensor-B	Sensor-C	Sensor-D
Capacity	200 kPa (2.039 kgf/cm^2)			
Rated output	1mV/V (=2000×10^6 strain) ± 20 %			
Safe excitation	3V			
Sensitivity	0.718 mV/V ± 1 %		0.748 mV/V ± 1 %	
Input & output Resistance	350 Ω ± 10 %			

*Note: 1mV/V corresponds to 2000×10^{-6} equivalent strain

Table 2 Median grain diameter of sediments (mm)

Type	G1	S1	S2	S3	S4	S5	S6
D_{50}	10.0	4.26	2.56	1.85	0.94	0.67	0.29

Table 3 Properties of bed sediment material

Sediment	D_{50} (mm)	D_{max} (mm)
Sediment-A	1.783	10.871
Sediment-A	2.304	11.142

acrylic planks 10 mm thick. To generate the debris flow, a section of the flume (2.8 m upstream from the outlet) having dimensions 1.9 m long and 7 cm deep is filled with the sediments supported at the downstream by a 7 cm high weir. The reason behind the installation of weir at the downstream of the debris flow generation section is to make the sediment pre-saturated before the debris flow generation. Then the debris flow is generated overflowing the installed weir. As for the sediment used in the experiments, silica sands (S1, S2, S3, S4, S5, S6) and gravel (G1) were mixed in equal proportion by weight to prepare the bed sediment-A. Silica sand (S1, S2, S3, S4, S5, S6) in proportion (1.6, 1.5, 1, 1, 1, 0.7) and gravel (G1) in (1.7) by weight were mixed to prepare the bed sediment-B. Table 2 shows sediments with median grain diameters and

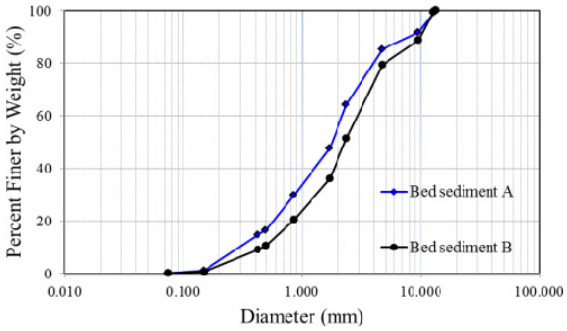

Fig. 5 Particle size distribution curves

properties of sediment material are shown in Table 3. Fig. 5 shows particle size distributions of the prepared material for bed sediment A and bed sediment B. The bed sediments have an angle of repose, $tan\phi$ = 0.7 and sediment density σ = 2.65 g/cm^3 and are saturated with water. Debris flow is produced by supplying a constant water discharge of 300 cm^3/sec for 10 sec from the upstream end of the flume. Details of the experimental setup are shown in Fig. 6.

To measure the approaching velocity of debris flow in this study, a high-speed camera was installed at the front of dam. The flow was filmed with a high-speed camera (Casio: EX-ZR300) placed on the side and top of the channel (as shown in Fig. 6). A powerful imaging technique is exploited to measure the tracer velocities and flow patterns. At the chosen video rate of 480 frames per second, the digital images have a resolution of 224×160 pixels. Fig. 7

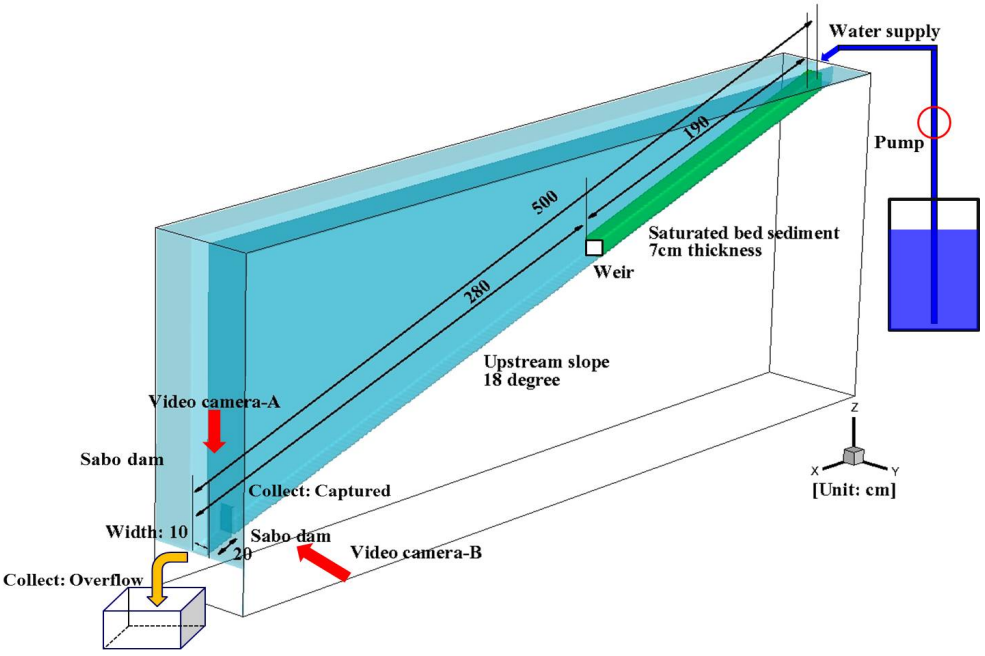

Fig. 6 Sketch of experiment flume for debris flow

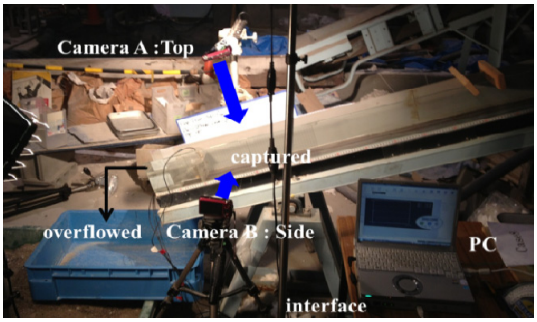

(a) Measuring system

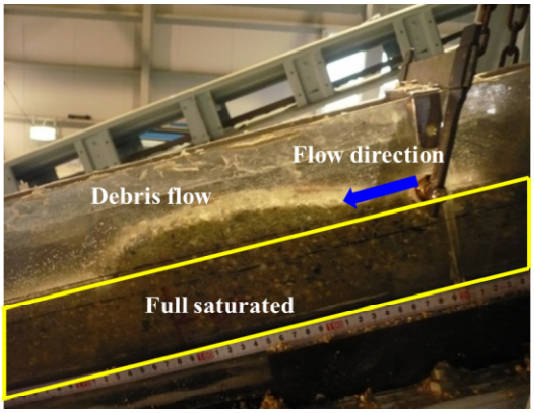

(b) Generation of debris flow at the upstream

Fig. 7 Experimental set-up for debris flow

shows the measurement systems and generation of debris flow at the upstream. The pressures data were sampled at frequency rates of 500 Hz, converted via an interface board and then recorded on a hard disk file.

The schematic diagrams of the three dams with different plans are shown in Fig. 8. The total pressure associated with major debris flows was recorded in real time by a system consisting of four sensors installed in the two different plans. The sensors were installed vertically along the flow depths (plan-1) and

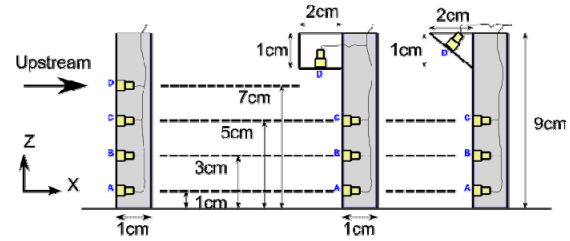

(a) plan-1

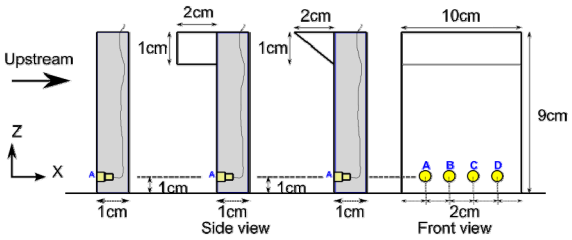

(b) plan-2

Fig. 8 Schematic diagram of three closed dams

horizontally at the same flow depth (plan-2). The uplift pressure and vertical distribution of total pressures were measured by plan-1 and the total pressure due to the impact collision was measured by plan-2. Furthermore, Table 4 and Table 5 show the experimental condition with both plans.

Debris flow velocity, the radius of the boulder and approaching height are very important factors to discuss the impact force. So far, to discuss the impact force of debris flow, there have been few experimental studies. Each experiment used three different generation methods. Itoh et al. (2011) explained the generation methods of debris flow as follows:

a) Type- NL: Natural landslide dam break.
b) Type-U: Sediment and water is supplied steadily in upstream end of channel.

Table 4 Experimental conditions for horizontal total pressure

Bed sediment	Sensor installation	Measurement	Repetition
A	Plan-2	Total pressure, velocity, depth	10 times
B	Plan-2	Total pressure, velocity, depth	10 times

Table 5 Experimental conditions for vertical total pressure

Type	Bed sediment	Sensor installation	Measurement	Repetition
Without flap	A and B	Plan-1	Total pressure	10 times
Flap-R dam	A and B	Plan-1	Total pressure	10 times
Flap-T dam	A and B	Plan-1	Total pressure	10 times

c) Type-QS: Bed sediment is set on the bed in upstream reach of channel, saturating upstream sediment with water, and supplying to input discharge from upstream.

In most studies, type-U has been used for debris flow generation. In this study, the phenomenon of the debris flow is approximated by the type-QS generation method. As the generation type is QS, the sediment composition and degree of saturation might not be uniform throughout the sediment layer. Also, the standard size of the boulder cannot be measured when a debris flow hits on the obstacle. Therefore the experiments were repeated several times under identical conditions. Debris flow produced in the experiments is the stony debris flow type and the largest particles are accumulated in the forefront. To measure the thickness of deposition (i.e. the flow depth plus the deposition thickness in the process and final stage) accurately, the graduations are marked on the side of the flume.

4. Results and discussions

Fundamental experiments were conducted to investigate dam-break and debris-flow for improvement of functions of the sabo structure. Considering quantitative and qualitative results from the experiments, the characteristics of the proposed closed dams were discussed and summarized as follows:

4.1 Comparison of flow profile near the dam

In order to confirm the characteristics (flow profile and total pressure), firstly only two types of closed dams (without and with flap-R) under the two flow conditions i.e. the clear water flow and the debris flow were tested with plan-1. The experiments were conducted for both flow conditions in order to observe the energy dissipation phenomenon near the dam. In the case of dam without flap, after suddenly opening of the gate, the flow hit the dam body and whole flow move vertically upward and then some

Table 6 Results of surface velocity in both flows

Flow type	Surface velocity (m/sec)
Clear water	1.176
Debris flow-Sediment.A	1.218
Debris flow-Sediment.B	1.244

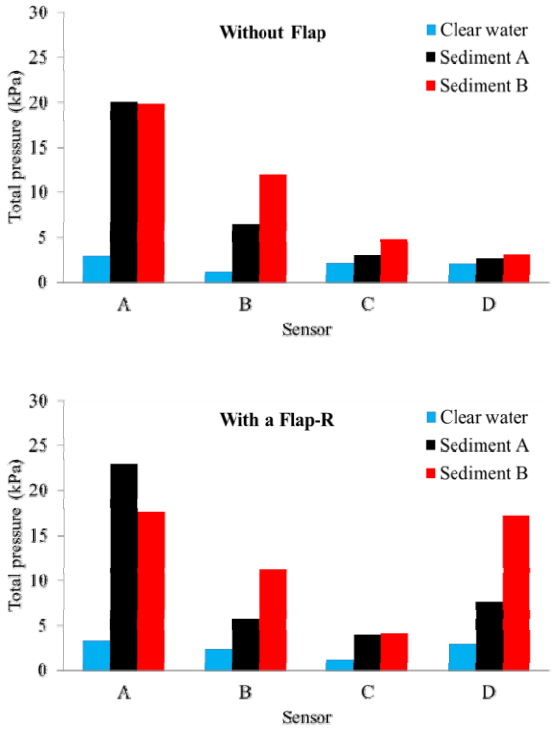

Fig. 9 Results of the total pressure due to clear water and debris flow

flows overtopped the dam while rest falls down upstream. But in the case of dam with flap, after hitting the dam surface by the flow, the flow moves towards the below part of the flap vertically. Then, the flap reflect back the flow upstream which looks like a bore traveling toward the upstream direction. The flow pattern with debris flow was observed without considering the flap structure. In such case, the flow pattern is similar to clear water case but due to the mixture of different size of sediments in the debris flow, we observed that some portion of the debris flow overflows carrying large sediments while rest of the flow remains upstream depositing remaining particles at the bottom part of the dam. In contrast, if we consider the flap structure, almost all the particles were captured and deposited upstream of dam due to the reflection from the flap.

Table 6 shows the average values of the surface velocities measured for different flow conditions (i.e. clear water and debris flows) in front of dam by a high-speed camera. Although the flow pattern and the approaching surface velocity are very similar, the total pressure is entirely different in both flow cases as shown in Fig. 9. This is due to the fact that the debris flow has a huge energy in the front part of the

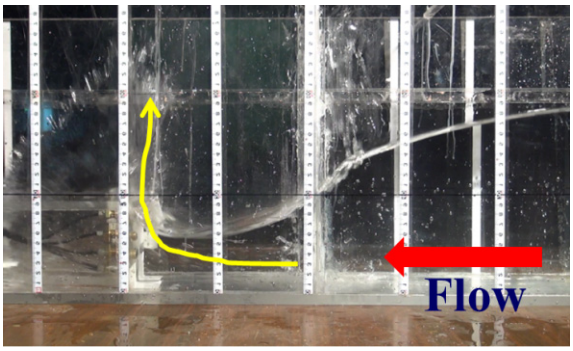

(a) Clear water case without flap

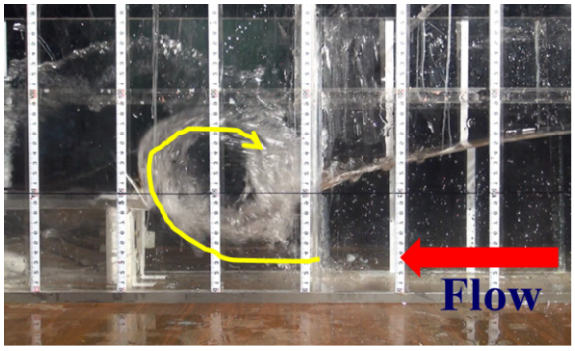

(b) Clear water case with flap-R

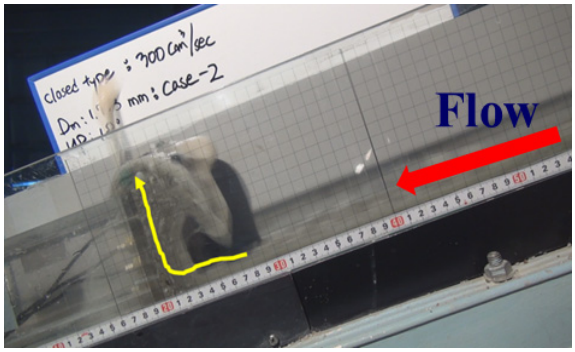

(c) Debris flow case without flap

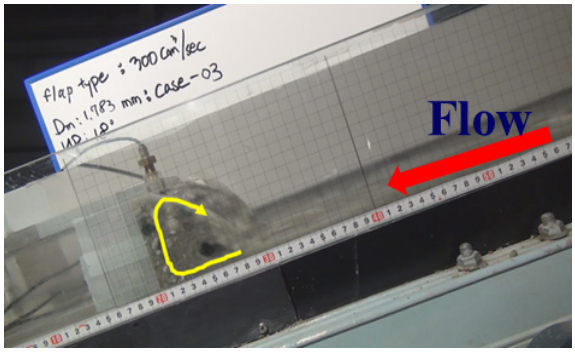

(d) Debris flow case with flap-R

Fig. 10 Results of the flow pattern for two different types of dam due to clear water and debris flow

flow that is much greater than clear fluid flow because of the accumulation of large boulders at the front.

Fig. 10 shows the test results of the flow pattern for two different types of dam in the case of clear water and debris flow. The flow patterns in the case of clear water flow are shown in Fig. 10 (a) for the dam without flap and the Fig. 10 (b) for the dam with flap-R dam whilst Fig. 10 (c) and (d) correspond to the debris flow condition for both types of dam. An important point is that each flow pattern is very different for each different type of dam but the pattern is the same in both flow cases. However, it shown that flap-R dam generated a larger volume of spray than the dam without flap downstream in both cases. A comparison of the total pressures due to the impact collision (i.e. the value is taken as the average of the total measured maximum value of pressure for each sensor in the number of experiments) reveals the following important points:

(1) The sensor D indicated nearly similar total pressure in both types of flow for the dam without flap (as shown in Fig. 9). The reason for this similarity is that, in both the flow cases, the movement of flow at the top of the dam (where sensor D located) is vertical i.e. most of the forces are uplift (due to the vertical nature of flow at the top as shown in Fig. 10 (a) and 10 (c)) and the dam without flap has no capability to absorb the uplift force since it has no flap. But the total pressures in the case of sensor A with debris flow have increased nearly 7 times in comparison to other types because at the bottom part of the dam (where sensor A is located) the debris flow has more impact force due to the sediments than the clear water since the flow here is not completely vertical as in sensor D as shown by Fig. 10 (b) and 10 (d).

(2) In the case of dam with flap-R, the values of sensor D with bed sediment B indicated that the total pressure has increased nearly 6 times in comparison to the clear water type and sensor A shows a 5 times increase in the value of total pressure. The reason for the increase in value is that the flap structure for debris flow absorbed higher uplift pressure than the clear water obviously and the bottom part has not changed significantly from point (1).

The above result shows that the dam with flap-R can reduce the quantity of spray transportation more efficiently than the dam without flap due to the flow profile so that the reduction in energy and overtopping time occurs. This experiment should also help us better understand the energy dissipation

process involved in the flow weakening. Even if the flap structure was shocked by the uplift pressure, it shows that the newly designed check dam with flap has the advantage of changing the total pressure compared to the dam without flap due to generation of the reflected flow. Furthermore, this result shows that the dynamic force of debris flow due to the impact collision is much greater than the clear fluid of dynamic force in comparison to the total pressure in the flow due to the average of maximum total pressure.

4.2 Debris flow experiment

Debris flow experiments were conducted using two types of bed sediment in order to check the efficiency of all three types of dam under consideration namely without flap, with flap-R, and with flap-T. All experiments measured the total pressure using a measuring system. As a generation of Type-QS, the sediment composition and degree of saturation might not be uniform throughout the sediment layer. So the data obtained from experiments repeated several times under the same hydraulic conditions were used for data analysis. In the experiments, in order to test if the average of the total pressure (by the maximum value for each case) is statistically significant with different types of dam, as well as to remove the outlier data from the original data, we used graph analysis with a boxplot method. A boxplot is a device used to represent the median of the data, the upper and lower quartiles, and any data points that possibly are outside (outlier) values, and it is also useful for summarizing a data set.

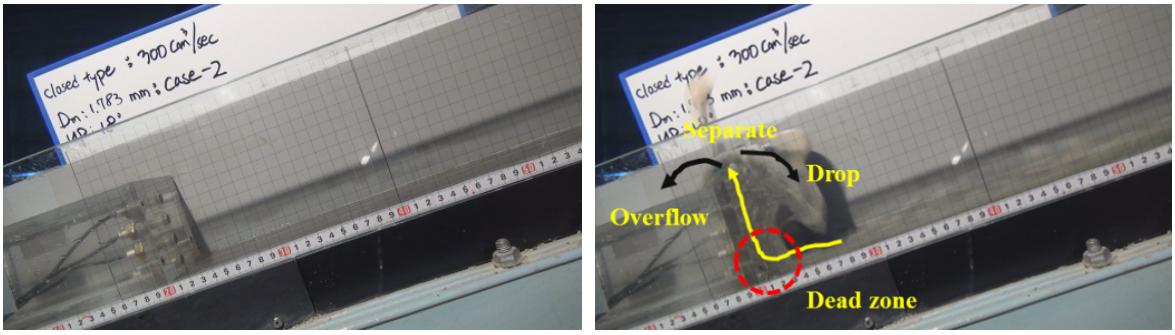

(a) Without flap: Initial condition, at t = 0.0sec At time = 6.67sec

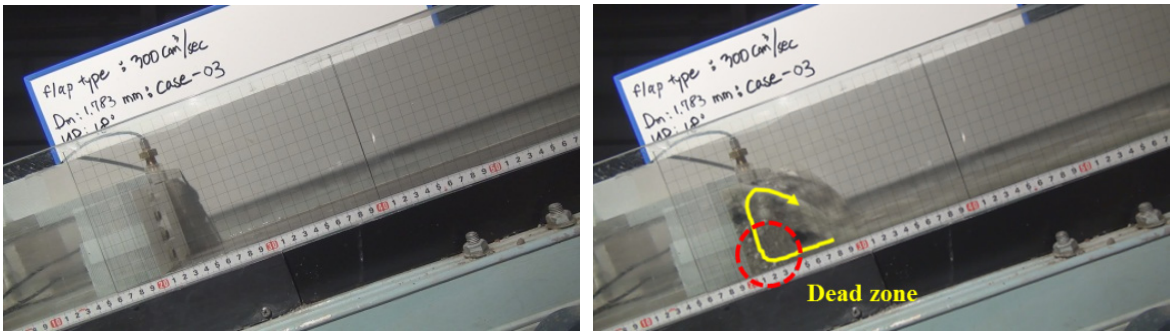

(b) With flap-R: Initial condition, at t = 0.0sec At time = 7.43sec

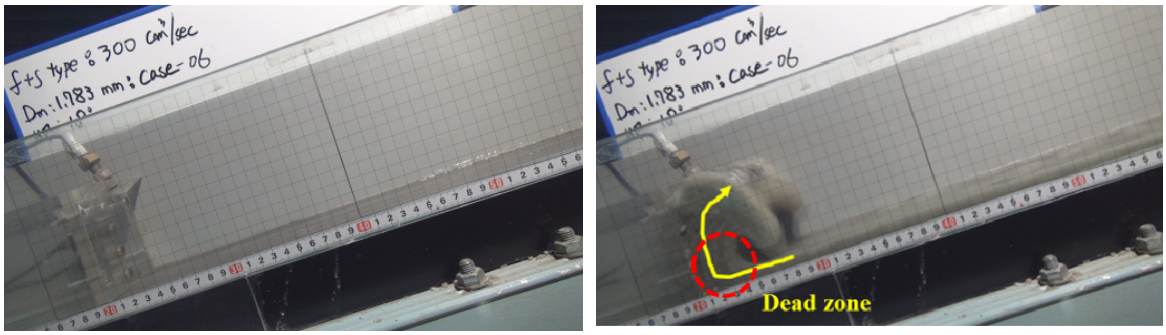

(c) With flap-T: Initial condition, at t = 0.0sec At time = 6.30sec

Fig. 11 Movement of debris flow at different time step: sediment A

4.2.1 Flow pattern

Fig. 11 shows the characteristics of debris flow movement in case of all three types of dam (i.e. a: without flap, b: with flap-R, and c: with flap-T) at different time steps. The figure clearly reveals that, in the case of a dam without flap, the large particles are seen to overflow whereas in other two types of dam such particles are seen to be captured. This leads to the conclusion that flap-T and flap-R types are more efficient regarding the capturing of large debris mass. This is because the flap structure is more efficient in capturing the large particles. The flow patterns of the proposed dams obtained by the experiments are described briefly as follows:

(1) In the case of a dam without flap: the flow pattern is influenced by the characteristic of debris flow (especially the approaching flow depth and velocity). First the dam was immensely shocked by the impact collision; secondly flow uprush occurred vertically with large boulders due to the uplift pressure quickly and finally the debris flow separated into two flows at the top of the dam: some debris flow is transformed as an overflow with few large boulders, and other debris is dropped by gravity from the top of the dam. A dead zone is developed at the bottom of the dam by the incoming debris flow simultaneously with the above process. Due to those processes, now the channel bed will rise upstream of the dam because of the captured debris mass.

(2) In the case of the proposed dams (i.e. flap-R and flap-T dams), when debris flow occurs in front of the dam, the impact collision and the vertical lift of the debris mass occur in similar fashion as in the case of the dam without flap but there will be no overflow of the debris mass and all the debris mass is captured upstream of the dam due to the generation of the reflected flow as shown in Fig. 11 (b) and Fig. 11 (c). But later after deposition above the dam height the overflow of debris mass may occur. Therefore, it is inferred from this process that the proposed dam type will capture more large boulders than the other types of dam and also the proposed type will reduce the overflow time (which is not quick enough like the dam without flap) and reduce the impact energy on the dam from the incoming debris flow due to the deposited mass before the dam.

Although the figure shows that the final stage of the debris flow pattern is similar in all three types of dam, it should be understood that the process to reach the final stage is different for each type of dam as shown by the research.

4.2.2 Vertical distribution of total pressure

To estimate the external force of flap structure, the vertical distributions of total pressure for the three dams under the two different bed sediment conditions are investigated (Table 5 shows the experimental conditions).

Table 7 compares the test results on the average of maximum total pressure values by plan-1. Proposed closed dams are the extension of a typical vertical dam with flap installed at the top. But, this might be vulnerable to accidental bumps due to the uplift pressure. In order to check the uplift pressure, sensor D was installed within the flap. The results obtained by comparing the total pressure and uplift pressure are summarized as below:

(1) In the case of sediment A: the uplift pressure of the flap-R dam has increased by nearly 3 times in comparison to other types. The reason for this increase is that the rectangular type has to absorb all of the uplift pressure directly while the flap-T type has more smooth control due to its shape and the typical type has no flap at all.

(2) In the case of sediment B: even if the main total pressures due to the impact collision are very similar by the value of sensor A, the values of uplift pressure for the flap-R type have increased by nearly

Table 7 Results of total pressure without outlier data (unit: kPa)

	Sediment A			Sediment A		
	Without	Flap-R	Flap-T	Without	Flap-R	Flap-T
Sensor-A	20.014	22.880	16.090	19.850	17.614	19.397
Sensor-B	6.478	5.764	9.749	11.985	11.317	7.728
Sensor-C	3.003	3.891	4.128	4.704	4.055	6.596
Sensor-D	2.689	7.645	2.611	3.120	17.199	0.492

35 times in comparison to other types. So the flap-T type is still efficient in comparison to the flap-R type regarding uplift pressure. Therefore, the flap-T type can more effectively control the uplift pressure than the flap-R type due to generation of the reflected flow. Even if both flap types were shocked by the uplift pressure, it shows that the newly designed check dam with flap has the advantage of changing the dynamic pressure compared to the dam without flap due to generation of the reflected flow.

Fig. 12 shows the trend line of vertical distribution of total pressure using the average of maximum values for the three dams (as shown in the dotted line) and the trend line (as shown in the black line) without the uplift pressure for both dams (i.e. flap-R and flap-T dams by sensor D) are estimated by the following relation:

$$x = Me^{Ny} \tag{8}$$

where x: total pressure, y: height of dam, and M and N are constant coefficients. The results obtained by comparing the trend line of vertical distributions are summarized as below.

In the case of sediment A and B, all dam types show a similar trend of vertical distribution of total pressure. However, the flap-R dam shows two patterns regarding the vertical distribution of total pressure (i.e. the first pattern is decrease from bottom to below the flap part; the second pattern is rapid increase at the flap part due to the uplift pressure). This is because the flap-R type has to absorb all of the uplift pressure directly. So, it shows the effectiveness of adding the rectangular flap to the conventional dam. But the flap-T shows a similar trend to the dam without flap due to the fact that it has a smooth control of the pressure because of its shape. So, the pressure calculation while designing the sabo dam with flap-T does not require any different approach to that of the without flap dam but the flap-R does require a different approach for the consideration of uplift force.

4.2.3 Mass ratio of debris

To clarify the function of flap structures, the captured and overflowed sediment of debris flows between the without and with flap-T dams under the

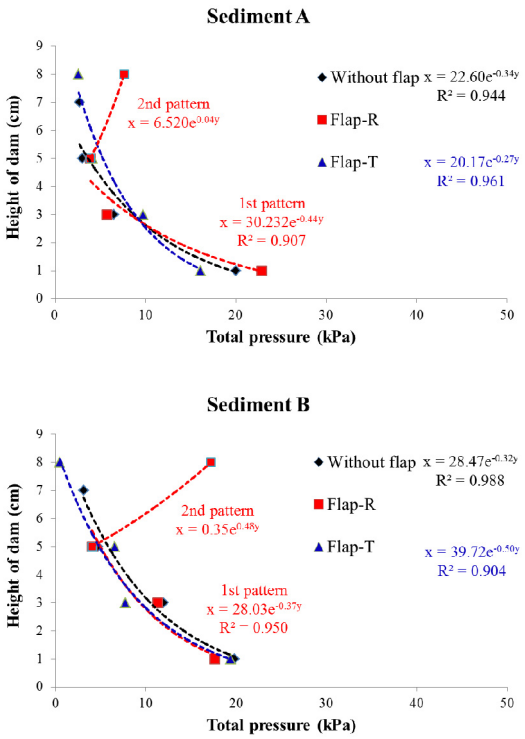

Fig. 12 Vertical distribution of total pressure for three dams

two different sediment conditions were observed. The experiments were repeated 5 times under identical conditions. The mass of debris (i.e., the overflow and captured) were measured directly at the final stage by an electronic scale. After the generation of debris flow, the bed sediments remained in the upstream end of the flume. In both cases of sediment A and B, the generation of debris flow mass was calculated for without and with flap-T cases by summing up the captured and overflow mass of debris. Initially for the experiment, the sediment (density of 2.65 g/cm^3 and porosity of 0.35) of about 23 kg was fed through the channel. Table 8 compares the test results regarding the overflow, captured and generated, of the debris mass for the three dams. Out of 23 kg mass for generation of debris flow, the actual generation of debris flow as measured by summing of the captured and overflow debris flow mass was found to be 37.60 % of the total (8.648 kg) for sediment A and 39.62 % of the total (9.114 kg) for sediment B in the case of without flap dam. The results indicate that a similar quantity of debris flow was generated during the experiment. For the flap-T type also, the recorded values of actual generation of debris flow were 38.13 % and 35.95 %, respectively for sediment A

Table 8 Results of total pressure without outlier data (unit: kPa)

	Sediment A		Sediment B	
	Without flap	With flap-T	Without flap	With flap-T
Overflow (kg)	2.116	2.570	1.245	1.397
I (%)	24.44	29.23	13.73	17.48
Captured (kg)	6.532	6.119	7.868	6.872
II (%)	75.56	70.77	86.27	82.52
Generated (kg)	8.648	8.769	9.114	8.269
III (%)	37.60	38.13	39.62	35.95

*I: comparing the mass between generated and overflow

*II: comparing the mass between generated and captured

*III: comparing the mass between generated and input sediment

*Input sediment mass at upstream for generation of debris flow = 23 kg

and sediment B cases. Based on this result, we concluded that there is very good reproducibility of the tests, giving confidence in the results obtained by applying the generation method of debris flow.

4.2.4 Median grain diameter

Table 9 shows the median diameter of sediments for dams of without flap and with flap-T under two different sediments. The results obtained by comparing the captured and overflow debris mass grain size distribution for three stages with two different check dams are summarized below:

(1) Bed sediment A: The median size of particles (d_{50}) of overflow debris mass increased by nearly 11 % compared to the generated debris flow median size for the case of the dam without flap. But, in the case of the dam with flap-T, nearly 4 % decrease in median size was observed. These results conclude that the flap structure will capture more debris mass than the without flap since less overflow means more capture. So flap-T type is more efficient to capture large debris mass than the without flap.

(2) Bed sediment B: The median size of particles (d_{50}) of overflow debris mass increased by nearly 17 % and 5 % compared to the generated debris flow median size for the case of the dams of without flap and with flap-T, respectively. These results conclude that even though the median grain size increased for both dam types, the percentage increment for the flap-T type is smaller compared to the dam without flap. The flap-T type is still efficient in comparison to without flap regarding the capture of debris mass.

4.2.5 Force behavior of debris flow

The force behaviour of debris flow can be classified into three stages. The maximum total pressure will occur due to the impact force (by the collision) when debris flow just reaches the sabo dam at first. Secondly, both the dynamic and static applying condition will occur due to moving debris flow. Finally, the static applying condition will occur due to the static pressure when debris flow is deposited on the front of the sabo dam. Fig. 13 as the case of the flap-R dam shows the movement of debris flow due to the main forces for each stage condition.

Fig.14 shows the variation of total pressure due to the main applying force with time. The debris flow in front of the dams became strongly turbulent due to

Table 9 Results of the median grain diameter (d_{50})

	Sediment A		Sediment B	
	Without	Flap-T	Without	Flap-T
Overflow (mm)	2.201	1.658	3.330	2.853
I (%)	(▲) 10.5	(▼) 4.3	(▲) 16.6	(▲) 5.4
Capture (mm)	1.931	1.789	2.764	2.669
II (%)	(▼) 3.1	(▲) 3.2	(▼) 3.3	(▼) 1.4
Generated (mm)	1.992	1.733	2.857	2.707

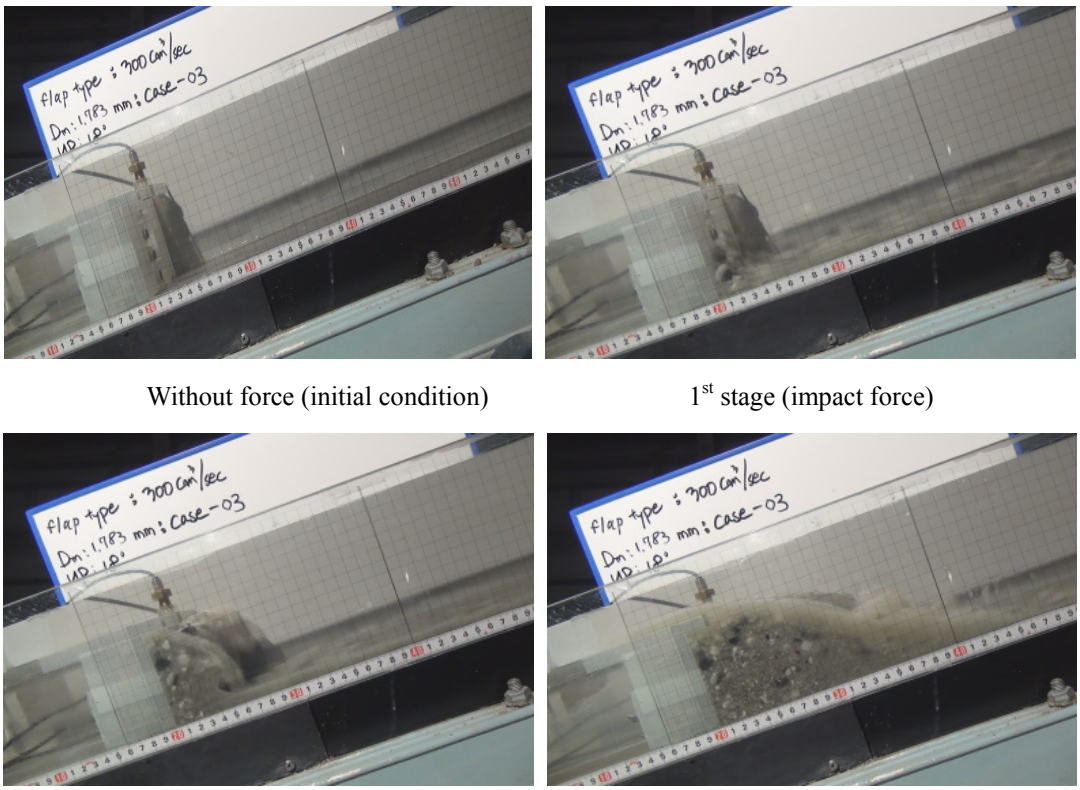

Without force (initial condition) 1st stage (impact force)

2nd stage (dynamic and static forces) 3rd staged (static force)

Fig. 13 Movement of debris flow due to main forces with bed sediment B (Flap-R dam)

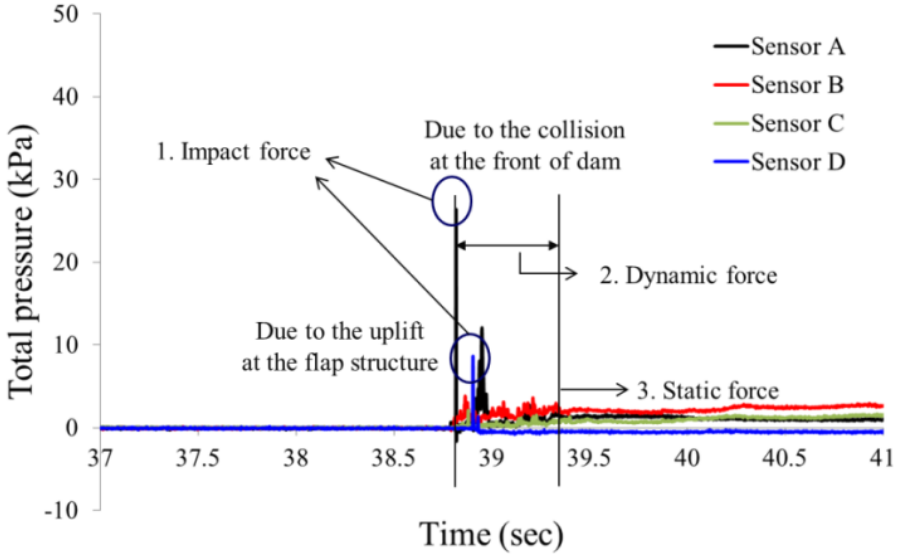

Fig. 14 Variation of total pressure due to the main forces with bed sediment B

the impact (stage: 1), dynamic (stage: 2) and static (stage: 3) forces that are shown by the sharp increase in the value in the graph shown in the figure. After the debris flow stopped, the static pressure was the main force since the debris mass has deposited in front of the dams and the depth of water has increased.

4.2.6 Impact pressure and velocity

To clarify the impact pressure due to the impact collision, parameters such as total pressure, approaching velocity and depth are observed during experiment. In the experiments, the data were obtained from the 10 times repeated experiments under the same hydraulic conditions with plan-2

Table 10 Results of the total pressure and surface velocity

	Sediment A		Sediment B	
	Total pressure (kPa)	Surface velocity (m/sec)	Total pressure (kPa)	Surface velocity (m/sec)
Q1	19.176	1.151	23.940	1.130
Median	37.621	1.231	33.011	1.231
Q3	59.136	1.272	73.477	1.338
IQ range	39.961	0.120	49.538	0.208
Average	42.415	1.218	43.512	1.244
Max	88.255	1.333	117.644	1.548

*Q1: Lower quartile
*Q3: Upper quartile
*IQ Range: Range of Q1~Q3

(Table 4 shows the experimental conditions).

Since plan-2 consists of sensor installation at the bottom part only, the results are extraneous as to dam shape but the values are directly connected to the bed sediments. Therefore, this experiment can obtain four values of the total pressure per one case and averages of the maximum values observed are used for the data analysis. Also, the box plot method of data analysis is performed as shown in Fig. 15.

Table 10 shows the test results for the averaged total pressure and surface velocity of debris flow under the two bed sediments. It shows that there are almost similar values of the average total pressures and velocities in the case of both bed sediments. However, in the case of bed sediment B, the maximum total pressure value has increased by nearly 1.3 times and Q1 (lower quartile) and Q3 (upper quartile) values have also increased by 1.2 times in comparison to sediment A. This should not be ignored. The reason for this increase is that the amount of large particles in the composition of sediment B is more than that of sediment A and maximum pressure is the result of sudden impact by the large particles. From this result, it is concluded that the maximum total pressure generated by debris flow is not proportional to the amount of debris flow, but strongly depends on the particle size distribution of debris flow. In addition, the results reveal that the colliding total pressure is different in all three types of dam although all the influencing parameters as described by Hu et al. (2011) such as generation pattern, initial sediment size, properties and volume, impact angle etc. are similar. The reason for this is due to the contact area of the sediment particles with the sensor. So the contact area of the different particles should be one of the important parameters when deciding impact pressure on the dam.

4.2.7 Impact model of debris flow

Pressure is the force on an object that is spread over a surface area. The equation for pressure is the force divided by the area where the force is applied.

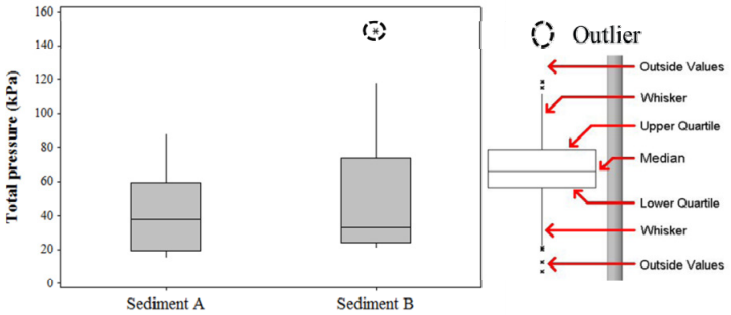

*lower quartile: split lowest 25% of data (= 25th percentile)
*upper quartile: splits highest 25% of data, or lowest 75% (=75th percentile)

Fig. 15 Results of the boxplot under the two bed sediments

Although this measurement is straightforward when a solid is pushing on a solid, the case of a solid pushing on a liquid or gas requires that the fluid be confined in a container. The force can also be created by the weight of an object. When we apply a force to a solid object, the pressure is defined as the applied force divided by the area of application. The equation for pressure is:

$$P = \frac{F}{A} \tag{9}$$

where P = the total pressure, F = the applied force, and A = the surface area where the force is applied. In this experiment, the total pressure from debris flow was measured by the dynamic pressure sensor. To calculate the applied force (i.e. impact force due to the collision) by Eq. (9), we have to estimate the actual contact area. But it is very difficult to obtain the actual contact area. So, in this study, the sensor area is considered as the actual contact area (A = 0.2826 cm^2). Likewise, Scheidl et al. (2012) also estimated the peak forces by multiplying measured pressure by the sensor contact area. To calculate the force of debris flow by Eqs. (3) and (5), various parameters such as the density of debris flow, the approaching surface velocity of debris flow, the flow depth, the discharge of debris flow, and the radius of the boulder are required. The approaching surface velocity of debris flow is obtained from the experiments by measurement from the high-speed camera. However, the flow depth is taken as average of 10 values of measurement of flow depth (= 2.0 cm), the radius of the boulder is obtained from the value of $d_{\max}$ from particle size distribution curves of gravel, and the discharge of debris flow was calculated from the channel geometry, approaching surface velocity, and depth of debris flow. Since the exact size of the colliding particles of debris flow (since it consists of variety of particle sizes) changes with time and the debris flow is accumulated with the large boulders at the front part of the flow, so for simplicity the maximum size of the particle is adopted for the calculations (i.e. 0.5 cm for sediment A and 0.6 cm for sediment B, refer Table 3). Finally, the density of debris flow is very difficult to measure in the flow through the experiment. So, the density of debris flow is calculated using an equilibrium sediment concentration equation. The equilibrium sediment concentration and the mixture density of debris flow are described as follows: According to Nakagawa et al. 2003, if a stony debris flow occurs ($\tan\theta_w > 0.138$), then

$$C = \frac{\rho \tan\theta_w}{(\sigma - \rho)(\tan\phi - \tan\theta_w)} \tag{10}$$

$$\rho_d = \sigma C + \rho(1 - C) \tag{11}$$

where ρ = the density of water, θ_w = the water surface slope, σ = the density of sediment particle, ϕ = the internal friction angle of the sediment, ρ_d = the mixture density of debris flow, and C = the sediment concentration of debris flow. The equilibrium sediment concentration is taken as 1.866 g/cm^3 calculated by Eq. (11) using the value of the density of sediment particles and water as 2.65 and 1 g/cm^3, respectively. The water surface slope is taken as 18º equivalent to the flume slope, and the angle of internal friction of the sediment is assumed as 35º. The results of impact force calculated using equations (3), (5) and (9) are shown in Table 11. This table shows the calculated applied force (i.e. due to the impact collision) of debris flow with different impact models for bed sediments A and B. The parameters of the equations are measured from the experiments under the same hydraulic conditions with plan-2 performing experiment 10 times. The maximum, minimum and average values for equations (3) and (5) in the table means the impact force is calculated using maximum, minimum and average flow velocities in 10 experiments while for equation (9) those values are calculated using maximum, minimum and average measured total pressure.

Furthermore, Table 12 shows a comparison of the empirical coefficients (i.e. pressure and force) used in both hydrodynamic and solid collision models with the experimentally obtained value from this study. The result shows the new range of values regarding the use of the equations of both models (i.e. hydrodynamic and solid collision model). The result from the experiment reveals that the values of k_p (i.e. coefficient of impact pressure) as proposed by other

Table 11 Results of the impact force with three theory (unit: N)

	Sediment A			Sediment B		
	Eq. (3)	Eq. (5)	Eq. (9)	Eq. (3)	Eq. (5)	Eq. (9)
Max.	6.632	1.701	2.494	8.944	2.931	3.325
Min.	4.649	1.375	0.425	3.891	1.779	0.591
Avg.	5.560	1.528	1.199	5.860	2.259	1.230
Parameters	ρ_d, v, Q	v, R	A	ρ_d, v, Q	v, R	A

Table 12 Comparison of empirical coefficients

Empirical coefficient			Sediment A	Sediment B
Hydrodynamic model	k_p by Eq. (2)	In this study	0.1~0.2	0.1~0.2
		Bugnion et al. (2001)	0.4~0.8	
	k_f by Eq. (3)	In this study	5.5* (1.9~11.8)	6.5* (1.8~12.6)
		Yamamoto et al. (1998)	1.0	
Solid collision model	k_f by Eq. (5)	In this study	1.8* (0.6~4.0)	2.5* (0.7~4.4)
		Mizuyama (1979)	1.0	

( ): Range value from experimental data

*: Average value

researchers are relatively smaller for the hydrodynamic model, but the values of k_f (i.e. coefficient of impact force) as proposed by other researchers are comparatively higher for both the hydrodynamic and solid collision models.

5. Results and discussions

In all the experiments, the effects of sabo structures, with emphasis in the sabo dams, the parameters such as the flow pattern, the surface velocity between the debris flow and clear water, the total pressure and the uplift pressure, mass ratio of debris, and median grain diameter were measured to compare the function of each sabo dam under the two different bed sediments. The empirical coefficients of the hydrodynamic and solid collision models are also determined and compared with available values of those coefficients. Furthermore, the characteristic of debris flow and proposed dams are confirmed due to the experiments. The experimental data analyses lead to the following conclusions:

(1) From the experimental results, although the flow pattern and the approaching velocity are very similar, the total pressure is entirely different in both flow cases. This is due to the fact that the debris flow has high energy in the front part of the flow, more than clear fluid flow because of big boulders accumulation at the front.

(2) The proposed closed-type sabo dams with flap structure can reduce the quantity of spray transportation more efficiently than the dam without flap (i.e. typical type).

(3) Flap-T type (triangle type) can control the uplift pressure more effectively than flap-R type (rectangular type) due to the generated reflected flow and is more efficient to capture large debris mass than the dam without flap (i.e. typical type). Even if both flap types were shocked by the uplift pressure, it was shown that the newly designed check dam with flap has the advantage of changing the dynamic pressure compared to the dam without flap due to reflection. Moreover, the triangular flap shows a similar trend like the dam without flap because it has smooth control of the pressure due to its shape. So, the pressure calculation while designing the sabo dam with flap-T does not require any different approach to that of the without flap dam but the flap-R does require a different approach for the consideration of uplift force. Therefore, the triangular flap structure is more suitable than the rectangular shape for actual application.

(4) The results of mass ratio of debris indicate that the similar quantity of debris flow was generated during the experiment. For the dams of without flap and with flap-T, the recorded values of the actual generation of debris flow were 38 % for sediment A and sediment B cases, respectively. From this result, it is concluded that the experiments revealed very good reproducibility of the tests, giving confidence in the results obtained by the applied generation method of debris flow.

(5) From the results of the median grain diameter, these results conclude that the flap structure will capture more debris mass than the dam without flap since less overflow means more capture. The case of sediment A shows the advantage clearly (i.e. the flap-T type is more efficient to capture large debris mass than the dam without flap). Even though the case of sediment B increased the median grain size for both dam types, the percentage increment for the flap-T type is small compared to the ordinary type. So, the flap-T type is still efficient in comparison to the ordinary one regarding capture of the debris mass.

(6) The force behaviour of debris flow can be classified into the three steps due to the main applied force (i.e. impact force, dynamic and static force, and static force).

(7) The empirical coefficients were estimated by the hydrodynamic and the solid collision models from the experimental results. The result from the experiment reveals that the values of k_p (i.e. coefficient of impact pressure) as proposed by other researchers are relatively smaller value for the hydrodynamic model but the value of k_f (i.e. coefficient of impact force) is comparatively higher for both the hydrodynamic and solid collision models.

(8) The maximum of total pressure generated by debris flow is not proportional to the amount of debris flow, but depends strongly on the particle size distribution of debris flow. Besides, the contact area of the different particles should be one of the important parameters when deciding impact pressure to the dam.

This study was carried out with the stony debris flow, but the case of mud debris flow proves equally applicable. The reason is that the mud debris flow is easy to generate and does not consist of larger particles compared to the stony debris flow. Also, the flap structure should build monolithically with main dam structure to correlate this research results.

Acknowledgements

This research is supported by JSPS AA Science Platform Program (Coordinator: H. Nakagawa) and support of Wakate fund program by Kyoto University Global COE Program (GCOE-ARS).

References

Armanini, A. (1997): On the dynamic impact of debris flows, In: Armanini A, Masanori M (eds) Recent developments on debris flows, lecture notes in earth sciences, Springer, Berlin, pp. 208-226

Bugnion, L., McArdell, B.W., Bartelt, P., and Wendeler, C. (2011): Measurements of hillslope debris flow impact pressure on obstacles, Landslides (2012) 9, pp. 179-187

Canelli, L., Ferrero, A.M., Migliazza, M., and Segalini, A. (2012): Debris flow risk mitigation by the means of rigid and flexible barriers - experimental tests and impact analysis, Nat. Hazards Earth Syst. Sci., 12, pp. 1693-1699

Hu, K., Wei, F., and Li, Y. (2011): Real-time measurement and preliminary analysis of debris-flow impact force at Jiangjia ravine, China, Earth Surface Process and Landforms 36, pp. 1268-1278

Huang, H.P., Yang, K.C., and Lai, S.W. (2007): Impact force of debris flow on filter dam, Geophysical Research European Geosciences Union, Vol. 9, 03218

Hübl, J., Suda, J., Proske, D., Kaitna, R., and Scheidl, C. (2009): Debris flow impact estimation, In: Popovska C, Jovanovski M (eds) Eleventh International Symposium on Water Management and Hydraulic Engineering, Vol. 1, pp. 137-148

Hungr, O., Morgan, G.C., and Kellerhals, R. (1984): Quantitative analysis of debris torrent hazards for design of remedial measures, Canadian Geotech. J., 21, pp. 663-677

Itoh, T., Horiuchi, S., Akanuma, J.I., Kaitsuka, K., Kuraoka, S., Morita, T., Sugiyama, M., and Mizuyama, T. (2011): Fundamental hydraulic flume tests focused on sediment control function using a grid-type high dam, Italian Journal of Engineering

Geology and Environment, B-114, pp. 1051-1061

Jackson, C.S.Y. and Do, S.C. (1969): Application of the Hertz contact law to problems of impact in plates, A report published by U.S. Naval ordnance laboratory white Oak, Maryland. (NOLTR 69-152)

Kim, Y., Nakagawa, H., Kawaike, K., and Zhang, H. (2013): Study on the function of a closed-type sabo dam with a flap for debris flow. 12th International Symposium on River Sedimentation, ISRS 2013 Kyoto. (In printing)

Larsen, M.C., Wieczorek, G.G., Eaton, L.S., and Torres-Sierra, H. (2001): The rainfall-triggered landslide and flash flood disaster in northern Venezuela, December 1999, Proceedings of the Seventh Federal Interagency Sedimentation Conference, pp. IV9-16.

Lichtenhahn, C. (1973): Die Berechnung von Sperren in Beton und Eisenbeton, In: Kolloquium über Wildbachsperren, Mitteilungen der Forstlichen Bundesanstalt Wien, Vol. 102, pp. 91-127

Mizuyama T. (1979): Computational method and some considerations on impulsive force of debris flow acting on sabo dams, J. of the Japan Society of Erosion Control Engineering, 112, pp. 40-43 (in Japanese)

Nakagawa, H., Satofuka, Y., and Kawaike, K. (2003): Numerical simulation of sediment disasters caused by heavy rainfall in camuri Grande basin, Venezuela 1999, Proceedings of the Third Conference on Debris-flow Hazards Mitigation: Mechanics, Prediction and Assessment, Switzerland Rotterdam, pp. 671-682

National Institute for Land and Infrastructure Management. Japan. (2011): Management of sediment-related risks, Associated program on flood management: 11

Okuda, S., Suwa, H., Okunishi, K., Yokoyama, K., Nakano, M., Ogawa, K., and Hamana, S. (1978): Synthetic observation on debris flow (part 4) observation in 1977, Disaster Prevention Research Institute Annals 21, Vol. 1, pp. 277-296 (in Japanese with English synopsis)

Pierson, T.C. (1986): Flow behavior of channelized debris flows, Mount St. Helens, Washington. In: A. D. Abrahams (ed.), Hillslope Processes, pp. 269-296 (Allen & Unwin, Boston).

Scheidl, C., Chiari, M., Kaitna, R., Müllegger, M., Karawtschuk, A., Zimmermann, T., and Proske, D. (2012): Analysing debris-flow impact models, based on a small scale modelling approach, Surv Geophys (2013) 34, pp. 121-140

Scotton, P., and Deganutti, A. (1997): Phreatic line and dynamic impact in laboratory debris flow experiments, In: Chen C (ed) Proceedings of the 1st. International Conference on Debris-flow Hazards Mitigation: Mechanics, Prediction and Assessment, American Society of Civil Engineers, New York, pp. 777- 786

Shibuya, H., Katsuki, S., Kokuryo, H., Ohsumi, H., and Ishikawa, N. (2012): Experimental study of load for steel frame check dam caused by debris flow with woody debris. Journal of the Japan Society of Erosion Control Engineering, Vol. 65, No. 1, pp. 54-61 (in Japanese with English Abstract)

Shieh, C.L., Ting, C.H., and Pan, H.W. (2008): Impulsive force of debris flow on a curved dam, International Journal of Sediment Research 23, pp. 149-158

Suwa, H., and Okuda, S. (1983): Deposition of debris flow on a fan surface, Mt. Yakedake, Japan, Z. Geo-morph, Vol. 46, pp. 79-101.

Watanabe, M., and Ikeya, H. (1981): Investigation and analysis of volcanic mud flows on Mt Sakurajima, Japan, Erosion and Sediment Transport Measurement (Proceedings of the Florence Symposium). IAHS Publ. No. 133, pp. 245-256

Yamamoto, A., Yamamoto, S., Toriihara, M., and Hirama, K. (1998): Impact Load on Sabo Dam due to Debris flow, Journal of the Japan Society of Erosion Control Engineering, Vo1. 51, No. 2, pp. 22-30. (In Japanese with English Abstract)

Zhang, S. (1993): A comprehensive approach to the observation and prevention of debris flow in China, Natural Hazards 7, pp. 1-23

(Received 11, June, 2013)